Title

Adaptation of the Tumor Antigen Presentation Machinery to Ionizing Radiation.

Journal

The Journal of Immunology, 211(4)

Authors

Lee, Mi-Heon
Ratanachan, Duang
Wang, Zitian
et al.

Publication Date

2023-08-15

DOI

10.4049/jimmunol.2100793

Peer reviewed

HHS Public Access

Author manuscript

J Immunol. Author manuscript; available in PMC 2024 August 15.

Published in final edited form as:

J Immunol. 2023 August 15; 211(4): 693–705. doi:10.4049/jimmunol.2100793.

Adaptation of the Tumor Antigen Presentation Machinery to Ionizing Radiation

Mi-Heon Lee[1], **Duang Ratanachan**[1], **Zitian Wang**[1], **Jacob Hack**[1], **Lobna Abdulrahman**[1], **Nicholas P. Shamlin**[1], **Mirna Kalayjian**[1], **Jean Philippe Nesseler**[1], **Ekambaram Ganapathy**[1], **Christine Nguyen**[1], **Josephine A. Ratikan**[1], **Nicolas A. Cacalano**[1], **David Austin**[2], **Robert Damoiseaux**[2,3,4,5], **Benjamin DiPardo**[6], **Danielle S. Graham**[6], **Anusha Kalbasi**[1,5,6], **James W. Sayer**[7,5], **William H. McBride**[1,5], **Dörthe Schaue**[1,5]

[1]Department of Radiation Oncology, Biostatistics and Radiology at the University of California, Los Angeles (UCLA), Los Angeles, CA, USA.

[2]Department of Molecular and Medical Pharmacology, Biostatistics and Radiology at the University of California, Los Angeles (UCLA), Los Angeles, CA, USA.

[3]Department of Bioengineering, Biostatistics and Radiology at the University of California, Los Angeles (UCLA), Los Angeles, CA, USA.

[4]Department of CNSI, Biostatistics and Radiology at the University of California, Los Angeles (UCLA), Los Angeles, CA, USA.

[5]Department of Jonsson Comprehensive Cancer Center, Biostatistics and Radiology at the University of California, Los Angeles (UCLA), Los Angeles, CA, USA.

[6]Department of Surgery, Biostatistics and Radiology at the University of California, Los Angeles (UCLA), Los Angeles, CA, USA.

[7]School of Public Health, Biostatistics and Radiology at the University of California, Los Angeles (UCLA), Los Angeles, CA, USA.

Abstract

Ionizing radiation (IR) can reprogram proteasome structure and function in cells and tissues. Here we show that IR can promote immunoproteasome synthesis with important implications for antigen processing and presentation and tumor immunity. Irradiation of a murine fibrosarcoma (FSA) induced dose-dependent *de novo* biosynthesis of the immunoproteasome subunits LMP7, LMP2, and Mecl-1, in concert with other changes in the antigen presenting machinery essential for CD8+ T cell-mediated immunity, including enhanced expression of MHC class I, β2M, TAP molecules, and their key transcriptional activator NOD-like receptor C5 (NLRC5). In contrast, in another less immunogenic, murine fibrosarcoma (NFSA) LMP7 transcripts and expression of components of the immunoproteasome and the antigen presentation machinery (APM) were muted after IR, which affected MHC-I expression and CD8+ T lymphocyte infiltration into NFSA tumors in vivo. Introduction of LMP7 into NFSA largely corrected these deficiencies, enhancing MHC-I

Corresponding Author: Dr. Dörthe Schaue, Department of Radiation Oncology, UCLA David Geffen School of Medicine, B3-109 CHS, 10833 Le Conte Avenue, Los Angeles, CA 90095-1714. Telephone: (310) 825-8246, FAX: (310) 206-1260, dschaue@mednet.ucla.edu.

expression and in vivo tumor immunogenicity. The immune adaptation in response to IR mirrored many aspects of the response to IFN-γ in coordinating the transcriptional MHC class I program, albeit with notable differences. Further investigations showed divergent upstream pathways in that, unlike IFN-γ, IR failed to activate STAT-1 in either FSA or NFSA cells while heavily relying on NF-κB activation. The IR-induced shift towards immunoproteasome production within a tumor indicate that proteasomal reprogramming is part of an integrated and dynamic tumor-host response that is specific to the stressor and the tumor and therefore of clinical relevance for radiation oncology.

Keywords

Immunoproteasome; LMP7; MHC-I; tumor infiltrating cells; irradiation; antigen processing

INTRODUCTION

Ionizing radiation (IR) as used in cancer radiation therapy (RT) is not only cytotoxic but it generates pro-oxidative and pro-inflammatory conditions with immunomodulatory potential (1). Of particular interest is its effect on MHC-I directed, antigen-specific CD8+ T cell responses that are critical for tumor immunity (2–4). Indeed, clinical studies have shown increased tumor-specific CD8+ T cell responses in patients undergoing RT, raising hopes that such responses may be leveraged by immunotherapy (5–8). In spite of this attention, only a few studies (9–12) apart from our own (13) have focused on the effects of RT on the antigen processing and presenting machinery (APM) that drives MHC-I directed tumor immunity. During this process, the 20S core of the proteasome produces peptides that are trimmed by proteasomal peptidases and inserted into the endoplasmic reticulum by transporters associated with antigen processing (TAP1/2) molecules. They may be further trimmed by aminopeptidases into typically 8–10 amino-acids with hydrophobic C termini that, assisted by chaperone proteins, such as calnexin, tapasin, ERp57, and calreticulin, are anchored in the MHC-I heavy chain cleft alongside β_2 microglobulin (β_2M) before being passaged to the plasma membrane for presentation to CD8+ T cells (14).

Proteasome structures display considerable architectural diversity that offers many options as to the quantity and quality of the antigenic repertoire that is generated. The basic 20S catalytic core is composed of four heteroheptameric rings that form a barrel-like structure with two outer rings of α-subunits that act as gatekeepers to control access of substrates to the two catalytic inner β-subunit rings. Various regulatory activators, such as 19S, PA28, and PA200, bind to one or both ends of the 20S core and, amongst other functions, open the pore to allow substrate entry (15). The ATP-ase dependent 26S ubiquitin-proteasome system has 19S regulatory particles bound to the 20S core (16, 17). Alternatively, PA28αβ, PA28γ, or PA200 bind to 20S cores to form ATPase- and ubiquitin-independent proteasomes that preferentially recognize oxidatively damaged or structurally unfolded regions on proteins and peptides (18). Hybrid proteasomes are also found with different activators attached to the same 20S core. The 20S core proteolytic standard proteasome subunits, X (ß5), Y (ß1), or Z (ß2) can be replaced by corresponding immunoproteasome subunits LMP7 (ß5i), LMP2 (ß1i) or Mecl-1 (ß2i) that are encoded within the MHC class II region adjacent

to TAP1/2 (19–21). Mixed 20S cores with standard and immunoproteasome subunits are also found. Cells within the immune system tend to express immunoproteasome subunits constitutively, though to varying extents, but immunoproteasome subunits can be induced in most cell types by pro-inflammatory, pro-oxidative conditions including under the influence of cytokines, in particular interferon-γ (IFN-γ) and tumor necrosis factor-α (TNF-α) (22, 23). All proteasome structures can generate immunodominant epitopes (24, 25) but immunoproteasome subunits are more efficient at cleaving substrates after basic and hydrophobic residues. The suggestion is that this produces antigenic peptides that are superior for binding MHC class I molecules for the stimulation of CD8+ cytotoxic T cells, and that limiting expression of immunoproteasome subunits to inflammatory tissue sites might limit the chances of autoimmune reactions (26). Importantly, cytotoxic T cells and expression of immunoproteasome subunits and other members of the APM, including NLRC5, are generally associated with better prognosis in multiple cancers (27) and with better response to immune checkpoint blockade (28).

IR is an oxidative stress for cells and tissues that generates pro-inflammatory, pro-oxidative conditions (1). We have shown previously that IR, even at low doses, yields a very rapid decrease in proteasome function in various normal and cancer cells (29) that is associated with loss of 26S structures (30). Proteasome structures relocate within the cell (31) and *de novo* synthesis of new proteasome structures is initiated that can include immunoproteasome subunits (13). Such findings suggest a novel mechanism by which RT might alter the recognition of tumor-associated rejection antigens by the immune system, contributing to its net effects on tumor immunity.

Cognizant of the limited literature in this field, our goal was to study IR-induced replacement of standard by immunoproteasome subunits, and other changes in the APM following IR and compare these to IFN-γ, which is an established driver of such responses, using a moderately immunogenic FSA fibrosarcoma and a weakly immunogenic, spontaneous NFSA fibrosarcoma, both originating in C3Hf/Kam mice (32, 33). IR and IFN-γ treatments induced expression of immunoproteasome subunits along with MHC-I and other members of the APM much more efficiently in FSA than in NFSA cells. The deficit in induction of LMP7 in NFSA cells was particularly striking, and not due to a mutation. Importantly, introduction of LMP7 into NFSA cells proportionally rescued MHC-I expression and enhanced tumor immunogenicity. We also demonstrate that IR differed from IFN-γ treatment in that it did not activate STAT1 in either cell line. Both treatments activated NLRC5 in FSA, which transcriptionally controls MHC-I and other genes involved in antigen processing and presentation, including LMP7 (27, 34) although the evidence suggests that NF-κB may be a critical requirement for IR-induced APM activation. These findings are important because detailed knowledge of the APM status in different cancers and how it is affected by RT would seem critical for optimizing its combination with immunotherapy. Since immunoproteasomes are superior at efficiently recognizing and removing oxidatively damaged, potentially toxic proteins (35, 36), immune adaptation to IR by proteasome structures might also act as a survival pathway (37) that could alter the tumor responses to RT directly as well as indirectly through the immune system.

MATERIALS AND METHODS

Mice

C3Hf/Sed/Kam and NOD/SCID/IL2r-γ^{null} (NSG) were bred and maintained in a defined-flora AALAC-accredited colony of the Department of Radiation Oncology at UCLA and used when 6 to 8 weeks-old. All procedures followed NIH animal care guidelines with IACUC approval.

Tumors and Reagents

FSA is an immunogenic methylcholanthrene-induced fibrosarcoma in C3Hf/He (C3Hf/Sed/Kam) mice (32), whereas NFSA is a poorly immunogenic fibrosarcoma that spontaneously arose in the same strain (33). These tumors have been extensively studied both radiobiologically and immunologically, where they do not cross-react (38). DC2.4 is a murine dendritic cell line gifted by Dr. K.L. Rock (UMass). FSA and NFSA, and DC2.4 dendritic cells were grown in Dulbecco's modified eagle medium (DMEM) and RPMI medium, respectively, supplemented with 10% fetal bovine serum (FBS) and 1% antibiotic-antimycotic solution (Corning Incorporated, Corning, NY, USA) at 37°C and 5% CO_2. Mouse IFN-γ was purchased from PeproTech (Rocky Hill, NJ, USA). All cell lines were tested and confirmed to be free of *Mycoplasma* using a PCR *Mycoplasma* Detection Kit (ABM, Richmond, Canada, cat. #G238). Unless stated otherwise, for tumor growth in vivo 5×10^5 cells in PBS were injected subcutaneously (s.c.) into the right thigh of each mouse and mean tumor diameters measured 2–3 times per week with Vernier calipers in two perpendicular dimensions.

Whole exome sequencing

Whole exome sequencing (WES) library construction was carried out using the KAPA Hyper Prep Kit (Roche, KK8504) followed by target enrichment with SeqCap EZ Share Developer Probe (Roche, 08333025001). Sequencing was performed with 150 bp pair-end run on Illumina Hiseq3000 instrument at UCLA's Technology Center for Genomics & Bioinformatics (TCGB) Core facility. The sequence data were aligned to the mm10 mouse reference genome using BWA v0.7.17. FreeBayes (version 1.0.1) was used for whole exome sequence variant calling with duplicated reads filtered beforehand and the variants annotated afterwards with RefSeq Transcripts 91.

Irradiation

For the in vitro irradiation, cells were plated at a density of 1×10^5 cells per well in 6-well culture dishes (Genesee Scientific, San Diego, CA, USA) overnight prior to irradiation using a Gulmay RS320 X-ray unit at 300 kV and 10 mA with 1.5 mm Cu and 3 mm Al beam filtration (Gulmay Medical Ltd., Surrey, UK) delivering 2–25 Gy at a dose rate of 2.8 Gy/min. Dosimetry used a Capintec ionization chamber calibrated to NIST standards and film (GAFCHROMIC EBT2, International Specialty Products, Wayne, NJ, United States). Tumors were irradiated in vivo using the same Gulmay irradiator when 6–9 mm in diameter. Mice were anesthetized by a single intraperitoneal injection of ketamine 100 mg/kg and xylazine 6 mg/kg and positioned on a Cerrobend jig with lead-shielding such that only

the right thigh with the tumor was exposed. Tumors were dissected 5–7 days later for downstream analyses.

Quantitative Real-Time PCR (qPCR)

300 μl of RNA lysis buffer (Zymo Research, Irvine, CA, USA, cat. #R1055) was added to each well in the 6-well plate for total RNA extraction using Quick-RNA MiniPrep (Zymo Research, cat. #R1055). cDNA synthesis was performed using the high-capacity RNA-to-cDNA kit according to the manufacturer's instructions (Applied Biosystems, Grand Island, NY, USA, cat. #4387406). Transcript levels were measured with the FastStart Universal SYBR Green Master Mix (Sigma-Aldrich, St. Louis, MO, USA, cat. #04913850001) by a CFX Connect thermal cycler (Bio-Rad, Hercules, CA, USA). Each reaction contained 1 μl of 10x diluted cDNA and 1 μl of primers in a total volume of 20 μl. The final concentration of all primers was 500 nM. Quantitative real-time PCR (qPCR) was performed with exon-junction spanning primers (Table I) and primer specificity validated based on thermal gradient and gel electrophoresis. Data were obtained in triplicates and normalized to glyceraldehyde 3-phosphate dehydrogenase (GAPDH) levels. mRNA expression is shown as $2^{-\text{delta Ct}}$ calculated using the equation: delta Ct (gene) = Ct (gene test) – Ct (endogenous control, GAPDH) with fold-changes to 0Gy mRNA when appropriate.

Analysis of Tumor-Infiltrating Immune Cells

Tumor single-cell suspensions were prepared from dissected tumors by enzymatic digestion in PBS containing 1 mg/ml collagenase D (Sigma-Aldrich, St. Louis, MO, USA, cat. #11088866001), 0.5 mg/ml Dispase II (Sigma-Aldrich, St. Louis, MO, USA, cat. #D4693), and 0.1 mg/ml DNAse I (Sigma-Aldrich, St. Louis, MO, USA, cat. #10104159001) with constant shaking for 30 min to 1 h at 37 °C. After removing large tissue debris, and passing through a cell strainer, the resulting suspension was washed with PBS (Corning Incorporated, Corning, NY, USA) and resuspended in PBS+2% BSA at 1–2 × 10^6 cells/ml. Single-cell suspensions were stained with BD Horizon Fixable Viability Stain FVS 510 (BD Biosciences, San Jose, CA, cat. #564406) for 15 min at room temperature in the dark. Cells were then washed with cold PBS+2% BSA and Fc block added (BD Pharmingen, San Jose, CA, cat #553142) for 5 min at 4 °C, prior to another 30 min incubation with one or more of the following fluorochrome-conjugated anti-mouse antibodies: Alexa Fluor 647 anti-H-$2K^K$ (BioLegend, San Diego, CA, cat. #114912), isotype control antibody (BioLegend, cat. #400234), Alexa Fluor 700 anti-CD45 (BioLegend, cat. #109822), BV605 anti-CD3 (BioLegend, cat. #100237), APC-Cy7 anti-CD4 (Tonbo Biosciences, San Diego, CA, cat. #25–0041), PerCP-Cy5.5 anti-CD8 (Tonbo Biosciences, cat. #65–0081), and anti-CD11b (Tonbo Biosciences, cat. #35–0112). Data were acquired using an LSRFortessa (BD Biosciences, San Jose, CA, USA) and analyzed using FCS Express 6 software (De Novo, Pasadena, CA, USA) (Supplementary Figure S1).

Western Blot Analysis

Cells in the 6-well plate were washed twice with ice-cold PBS and 50–70 μl PhosphoSafe Extraction Reagent (Millipore Sigma, St. Louis, MO, cat. #71296) added with a protease inhibitor cocktail (Sigma-Aldrich, St. Louis, MO, cat. # 05892970001). Cells were harvested by scraping and lysed by vigorous vortexing for 15 sec. Cell debris were removed at

20,000g for 20 min at 4 °C and supernatant protein concentrations determined using a BCA protein Assay Kit (Fisher Scientific, cat. #23227) with bovine albumin as standard. Equal amounts of protein (50–100 μg/lane protein from cell lysate) were separated in a 10% precast SDS-PAGE gel (BIO-RAD, Hercules, CA, cat. # 4561033) and transferred onto PVDF membranes (Thermo Fisher Scientific, cat. #88518). After incubation with 5% BSA in TBST (10 mM Tris, pH 8.0, 150 mM NaCl, 0.5% Tween 20) for 60 min, the membrane was washed once with TBST and incubated with anti-mouse antibodies against LMP7 (cell signaling, Beverly, MA, USA, 1:1000, cat. # 13635), pSTAT1 (cell signaling,1:1000, cat. #9167), STAT1 (cell signaling,1:1000, cat. #9172), and GAPDH (Advanced ImmunoChemical, Long Beach, CA; 1:10000, cat. #2-RGM2) at 4 °C overnight. Membranes were washed 3 times for 10 min and incubated with secondary antibodies of IRDye 800CW (LI-COR Biosciences, Lincoln, NE, USA; cat. #926–32210) or IRDye 680RD-conjugated anti-mouse or anti-rabbit antibodies (LI-COR Biosciences; cat. #926–68071) for 1 h at room temperature at a 1:10000 dilution. Blots were washed with TBST 3 times, and proteins were visualized on an Odyssey Infrared Imaging System (LI-COR Biosciences, Lincoln, NE, USA) with both 700 and 800 nm channels according to the manufacturer's protocols.

Construction of LMP7 Expression Vectors

The super piggyBac transposase expression vector and pB513B-1 transposon vector were purchased from System Biosciences (Mountain View, CA). All constructs were confirmed by DNA sequence analysis. pB_TAC_ERP2 (Addgene #80478) plasmid was used as recipient plasmid in Gateway reaction to make the final construct pB construct containing the LMP7 gene. The pB-LMP7 construct was generated by addition of attB1/B2 sites via PCR to the LMP7 gene (Supplementary Table I) and moved into the pB backbone via Gateway pB_TAC_ERP2 plasmid according to manufactures protocol (Figure 5). For transfection NFSA cells were seeded into a 6 well plate at 5×10^5cells per well using DMEM supplemented with 5% FBS, PSG and left to adhere for 24 hours. The cells were then treated with 100 ng of pB plasmid construct (either LMP7 or mCherry in pB_TAC_ERP2) complexed with Lipofectamine 3000 Reagent (Invitrogen) at 1:2 (μg/ μL) ratio along with 100 ng Super pB transposase vector (System Biosciences, Mountain View, CA), prior to incubation for 72 h. The transfected cells were then treated with 60 μg/ml puromycin for one week, and the survivors expanded for testing by treatment with 5ug/ml Doxycycline to induce gene expression. Expression of cell lines with mCherry only and LMP7-mCherry was confirmed via flow cytometry.

Immunogenicity testing

To prepare the tumor vaccine, WT NFSA and NFSA cells expressing LMP7, or control vectors were treated with doxycycline (dox; 0.2 μg/ml; Sigma-Aldrich, cat. #D989) for 3 days at 37 °C. Doxycycline was washed off with PBS and cells resuspended in saline at 5×10^6/ml before being lethally-irradiated with 25 Gy. 6–8-week-old C3Hf/Kam mice were immunized by intraperitoneal (i.p.) injection with 1×10^6 of lethally-irradiated tumor cells and challenged 10 days later by s.c. injection of 5×10^6 cells WT NFSA cells. Tumor growth was assessed 2–3 times per week as above.

siRNA treatment of FSA cells

1.5~2 × 10^5 FSA cells/well were seeded in 6-well plates in DMEM containing 10% FCS and 1% penicillin-streptomycin (P/S). On day1, cells were serum starved by changing to DMEM without FCS and P/S for 5hours prior to adding 20 nM siRNA and Lipofectamine 2000 (Life Technologies). siRNAs used were ON-TARGETplus SMARTPool siRNA™ against mouse NLRC5 (L-067620, Horizon Discovery), mouse LMP7 (L-048952, Horizon Discovery), and non-targeting Pool (control siRNA) (D-001810, Horizon Discovery)(RNA sequences listed in Table II). After overnight transfection, the media was changed to DMEM containing 10% FCS and 1% P/S for a further 48 h and 72 h incubation at 37 °C before harvest, RNA extraction and qPCR or for flow cytometry. Pharmacological inhibition of NF-κB was achieved using (20 μM) Caffeic acid phenethyl ester (CAPE) (Calbiochem, San Diego, CA, USA) known to block nuclear translocation.

CTL Assay

The percent of cytotoxic activity was measured using bioluminescent plate-based LDH release in vitro assay (LDH-Glo, Promega, Madison, WI, USA) according to manufacturer's instructions. C3H mice were immunized i.p. with 5×10^6 25Gy-irradiated NFSA-LMP7-mCherry cells that had been treated or not with DOX. Spleens were harvested 5 days later, and T cells enriched over nylon wool columns (Polysciences, Warrington, PA, USA) were used as effector cells. 2×10^4 effector cells/well were co-cultured with target cells at effector to target (E:T) ratios of 20:1 and 5:1 in opaque 96-well plates for 30 h in 200ml of RPMI+5% FBS containing IL-2(3000U/ml). NFSA, NFSA-mCherry+DOX, NFSA-LMP7-mCherry+DOX, and FSA cells served as target cells. Supernatants were collected, and diluted 100x in storage buffer (10% Glycerol, 1% BSA in 200mM Tris-HCl, pH 7.3). Maximum and spontaneous LDH releases were determined using supernatants from cells treated with 10% Triton X-100 and medium, respectively. The percentage of specific cytotoxicity was calculated using the following formula:

$$\%\,\text{Cyotoxicity} = \frac{\text{Experimental LDH} - (\text{Effector}_{\text{Spontaneous LDH}} + \text{Target}_{\text{Spontaneous LDH}})}{(\text{Target}_{\text{Maxumum LDH}} - \text{Target}_{\text{Spontaneous LDH}})} \times 100$$

Analysis of publicly available data

We obtained matched clinicopathologic and transcriptomic data from The Cancer Genome Atlas (TCGA) Genomic Data Commons (GDC) Data Portal repository in May 2018. The TCGA sarcoma cohort includes 256 untreated sarcoma samples which were collected retrospectively from multiple institutions following institutional review board approval. They were processed, molecularly characterized, and pathologically verified by the TCGA Biospecimen Core Resource at the National Cancer Institute, as previously described (39, 40). RNA-Seq raw counts from the Illumina HiSeq platform and preprocessed with HTSeq were used for downstream immune deconvolution analysis. We estimated the abundance of tissue-infiltrating immune cells using the transcriptome-based method MCP-counter (41), which estimates the relative abundance of various tumor immune microenvironment constituents (T cells, CD8 T cells, cytotoxic lymphocytes, NK cells, B lineage cells, monocytic lineage cells, myeloid dentritic cells, neutrophils, endothelial cells,

and fibroblasts). We estimated the abundance of tissue-infiltrating CD8+ T cells in 253 soft tissue sarcomas represented in the TCGA, including UPS (n = 50), dedifferentiated liposarcoma (n = 59), myxofibrosarcoma (n = 25), malignant peripheral nerve sheath tumor (n = 9), leiomyosarcoma (n = 100), and synovial sarcoma (n = 10). Samples were analyzed for the expression pattern of 13 genes involved in antigen processing and presentation vis-à-vis CD8+ T cell content according to the immune deconvolution algorithm MCP Counter and visualized in scatter plots (Figure 4A) with Pearson correlation and statistical significance (Supplementary Table II). Stepwise multivariable regression modeling was performed with or without LMP7 as the first independent variable using SPSS (see below).

Statistical Analysis

Samples were run in triplicates, and all experiments were performed at least two or three times. Data are shown as means +/− standard deviation using GraphPad Prism. Differences between treatment groups were evaluated with Student's t-test and one-way analysis of variance (ANOVA) with Tukey's or Games-Howell's posthoc multiple comparison tests depending on the Levene's homogeneity of variance test results. The robust Welch procedure was used to compare in vivo tumor infiltrates amongst treatment groups and between cell lines while differences in tumor growth were assessed by Fisher's exact test. IBM SPSS Statistics for Windows, Version 24.0. (Armonk, NY, USA) was used for data base management and statistical analysis at a 5% level of significance.

RESULTS

IR induces expression of immunoproteasome subunits in FSA but little if any in NFSA cells.

To determine if tumor irradiation could reprogram proteasome production towards immunoproteasomes, FSA and NFSA cells were irradiated with 0, 2 or 8 Gy and mRNA expression levels of proteasome components assessed by RT-qPCR daily over 6 days (Figure 1). Both FSA and NFSA had very low basal levels of the immunoproteasome components that are encoded both within (LMP7, LMP2) (42) and outside (Mecl-1) (43) the MHC, when compared to the corresponding standard X, Y, and Z subunits. In contrast, DC2.4 dendritic cells, which served as a positive control, had high basal expression levels of both types of subunits and changed little after IR exposure (Figure 1A). Irradiation of FSA tumor cells increased expression of all 3 immunoproteasome components in a dose-dependent manner. By 2–3 days, levels approached equivalence with constitutive subunits, a response that was sustained for several days, especially for LMP7. These changes are best illustrated by shifts in the ratio, or balance, of immuno-to-standard proteasome subunits with time (Figure 1B). In marked contrast, irradiated NFSA responded with hardly any LMP7 expression and low LMP2 and Mecl-1 responses. These data are summarized as $\log_2$-fold changes to 0 Gy in the form of a heatmap in Figure 1C.

Although full dose responses were not performed, the immunoproteasome responses by FSA cells to 8 or10 Gy IR, which were equivalent in the effects they produce, were only slightly inferior to those induced by IFN-γ (Figure 2A). The lack of LMP7 and poor LMP2 responses in irradiated NFSA were confirmed in this context, but surprisingly,

while LMP7 did not respond to IFN-γ, LMP2 responses were normal. The assembly of mature proteasomes is a complex process that is generally considered to be led by β5 or β5i precursors as chaperones, with proLMP7 (β5i) being much more efficient than its constitutive counterpart β5 at maturing LMP2/MECL-1 immunoproteasomes (44). We examined proLMP7 and mature LMP7 levels by western blotting (Figure 2B) to determine if differences in FSA and NFSA in response to IR or IFN-γ could be due to variation in proLMP7 protein. Very high protein levels (100μg) were loaded for these blots as levels of proLMP7 are always low, but IR elevated both precursor and mature LMP7 proteins in FSA but not in NFSA, even though IFN-γ caused a clear uptick in mature LMP7 protein signal in the latter without any detectable proLMP7. This preliminary evidence suggests that proLMP7 would be unlikely to drive the formation of IFN-γ- induced immunoproteasomes, although the strong IFN-γ- induced LMP2 response in NFSA seen in Figure 2A may result in mixed proteasomes with altered function, which would require further study. Of possible clinical relevance is the finding that IR given prior to IFN-γ did not interfere with immunoproteasomes induction in FSA and there was at least an additive effect (Figure 2C).

Defective LMP7 and LMP2 expression affects other members of the MHC Class I antigen presenting pathway.

Many molecules in addition to the immunoproteasome subunits influence antigen processing and presentation for CD8+ T cell-mediated immunity, most prominently PA28 α/ß, POMP1, MHC-I, β2M, TAP1/2, and NLRC5 because it is the key co-transactivator of genes involved in MHC class I pathway, β2-microglobulin (B2M), immunoproteasome components LMP2 and LMP7, and TAP1 (27, 34). We included 19S regulatory subunits PSMC1 and PSMD4 and PD-L1 in our analysis for their proximity to this pathway. All were examined for their IR- and IFN-γ-inducibility (Figure 3A and B). It should be noted that the overall higher basal and induced mRNA levels in FSA than in NFSA cells may reflect, at least in part, basic differences in the size of the proteasome compartment in these two cell lines, which can result from the high chaperone activity of pro-LMP7 (44). IFN-γ-inducible TAP1 and TAP2 are encoded within the MHC adjacent to LMP7 and LMP2 and were upregulated by IR in FSA cells, while NFSA cells gave relatively poor IR-induced responses (Figure 3). Irradiation of both FSA and NFSA induced PA28α and β, 11S regulatory components in a manner comparable to TAP1/2, although the increase in PA28β for FSA after 8 Gy just failed to reach statistical significance ($P<0.64$, Games-Howell). These are also IFN-γ-inducible but encoded *outside* of the MHC. β2M that stabilizes the cell surface expression of the MHC class I α-chain to allow peptide presentation was also IR-inducible in both cell lines, as was expression of the proteasome maturation protein, POMP, that is essential for proteasome biogenesis. In fact, β2M induction by IR was even more pronounced than by IFN-γ in FSA. The changes in 19S subunits, PSMC1 and PSMD4 after IR or IFN-γ treatment were minor and seem unlikely to be of much biological significance. In many aspects, irradiation of FSA mirrored IFN-γ treatment in stimulating components of the APM, but interesting differences between the two stimuli exist that surface especially in the NFSA. For instance, NLRC5 gene expression following IR or IFN-γ treatment was significantly enhanced in FSA but muted in NFSA, while IFN-γ -induced MHC-I, β2M, TAP-1 and TAP-2 responses in NFSA were less subdued (Figure 3A). The comparison

of FSA and NFSA and their response to IR and IFN-γ are summarized in a heatmap representation of the data (Figure 3B).

Links between LMP-7 and MHC class I cell-surface expression have long been established (45) and proteasome maturation is known to enhance surface MHC class I levels (44). Induction of mRNA by IR was not very prominent in either cell line (Figure 3B) but since many factors contribute to MHC-1 expression on cells, and with the pivotal role of MHC-I in antitumor immunity in mind (46), we used flow cytometry to determine surface MHC-I expression in FSA and NFSA after IR or IFN-γ treatment. In vitro cultured FSA cells up-regulated surface MHC-I expression in response to either treatment, whereas NFSA did not respond to IR but did to IFN-γ, reflecting the mRNA findings (Figure 3C). Similar data were obtained in vivo as cells extracted from FSA tumors grown in immunodeficient NSG mice 2 days after RT also had increased MHC-I expression, while cells from irradiated NFSA tumors did not (Figure 3D).

IR-induced immunoproteasome expression correlates with immune infiltration into tumors.

In general, immunoproteasome-deficient mice have impaired anti-tumor immunity activity (47). Analogously, human tumors expressing immunoproteasomes have a better prognosis (27), and they respond better to immune checkpoint blockade (28). TCGA data in Figure 4A and Supplementary Table II illustrate the strong relationship between expression of individual immunoproteasome subunits, the APM, and intratumoral CD8+ lymphocytes in sarcomas of different histological types. In addition, using stepwise multivariable analysis modeling with PSMB8(LMP7) forced in as the initial covariate we were able to raise the coefficient of determination (R^2) of predicting CD8 T cell infiltration to $R^2 = 0.563$ ($p = 0.02$) by incorporating 6 other independent predictors, namely TAP1, PSMB10(Mecl-1), CTSH, RelB, PSMB9(LMP2), and TAP2. Of note, one of the genes featuring strongly was RelB, i.e. pointing at potential NFκB involvement (see below, Figure 7) which was also true when the model was run without forced variable (PSMB10, TAP1, CTSH, RelB, and β2m, $R^2 = 0.550$; $p = 0.023$). Collectively, this supports the concept of immunoproteasome expression directly linking to intratumor immunity.

To investigate if IR-induced tumor immune infiltrates correlated with immunoproteasome induction, FSA and NFSA tumors growing s.c. in syngeneic C3H mice were locally irradiated and tumor infiltrates examined 7 days later. The findings were very similar whether total live cells or $CD45^+$ cells were used for analysis, as can be seen by the presentation of both for CD4+ and CD8+ lymphocyte populations in Figure 4B. $CD4^+$ T cell representation was low in both tumors and increased only slightly after IR. In contrast, $CD8^+$ T cells were far more numerous in FSA than NFSA tumors at baseline and this difference was further accentuated following irradiation. In contrast, $CD11b^+$ myeloid cells were more numerous in NFSA than FSA tumors and did not change after treatment, except for a small decrease in irradiated FSA tumors (Figure 4B). Overall, the CD8+ T cell to CD11b+ myeloid cell ratios were much higher for FSA tumors, especially after treatment, while these ratios were very low for NFSA tumors at baseline and changed little after IR (Figure 4B). Notably, NFSA tumors grew slightly faster than FSA in vivo, and had less of

IR-induced tumor growth delay, as we have reported previously (38)(Supplementary Figure S1; includes the gating strategy).

Overexpression of LMP7 in NFSA enhances MHC-I surface expression, increases tumor immunogenicity, and inhibits tumor growth in vivo.

We explored the possibility that the dramatic deficiency in IR-induced LMP7 expression in NFSA might affect MHC-I expression and immunogenicity. This hypothesis was tested using a dox-inducible piggyBac LMP7 vector with a mCherry reporter gene to rescue LMP7 expression in NFSA cells (Figure 5A and B). As expected, LMP7 mRNA and protein levels were very low in the absence of dox, but became easily detectable after 3 days of dox treatment with an optimal concentration of 0.2 μg/ml, which coincided with LMP7 precursor expression and higher ratios of precursor-to-mature LMP7 protein (Figure 5C). LMP2 expression also increased, while Mecl-1 declined for unknown reasons and NLRC5 remained largely unaffected (Supplementary Figure S2). Importantly, LMP7 rescue consistently boosted mRNA and protein MHC-I expression on NFSA cells (Figure 5D), which correlated closely with mCherry reporter gene expression (Figure 5E).

Loss of LMP7 is a likely tumor immune escape mechanism and we hypothesized that expressing LMP7 in NFSA cells would have major consequences on their ability to grow in vivo. Indeed, $LMP7^{+}$ NFSA cells (NFSA-LMP7-mCherry) barely grew after injection and most were completely rejected by day 10, unlike parental NFSA tumors that grew progressively for 22 days (Figure 6A) and NFSA-mCherry control cells whose growth was slightly, but not significantly, delayed. To directly assess immunogenicity, mice were immunized with a vaccine of heavily irradiated NFSA, NFSA-mCherry, or NFSA-LMP7-mCherry and challenged with viable, parental NFSA cells 10 days later (Figure 6B). Immunization with NFSA unexpectedly slowed the growth of the tumor challenge, unlike previous experiments (38), which may have been due to time the cells spent in vitro during transfection, which was supported by the demonstration that in vivo passaged NFSA cells (“fresh” NFSA cells) were less immunogenic. Crucially, mice immunized with NFSA-LMP7-mCherry vaccine were unable to support the growth of parental NFSA tumors upon challenge, except for the brief appearance of one tumor on day 3, so all mice were tumor-free thereafter (Figure 6B left and Supplementary Table I). When these tumor-free mice were individually rechallenged with FSA and NFSA cells at different sites, FSA cells grew and NFSA cells were rejected in all cases (Figure 6B, right). This was recapitulated in an in vitro CTL assay using T cells from mice immunized against heavily irradiated NFSA-LMP7-mCherry cells. These more potently killed NFSA cells if LMP7 was expressed (Dox treatment) (Figure 6C) suggesting LMP7 expression made NFSA better as both stimulators and targets. These results support a role for LMP7 in tumor immunogenicity and tumor growth control.

FSA and NFSA responses to IR and IFN-γ diverge at the STAT1-NLRC5 junction.

Although the signaling mechanisms for the MHC-1 APM are complex and not the major thrust of this study, we explored whether the STAT1/NLRC5 axis is activated by IR, as it has been reported to mediate the response to IFN-γ (34, 48). Indeed, IFN-γ activated STAT1 in FSA cells within 10 min, which lasted for at least 1 h, whereas this was not

the case for NFSA cells that had very low STAT1 basal levels and was only minimally phosphorylated to pSTAT1 by IFN-γ (Figure 7C), which was in keeping with the lack of NLRC5 mRNA induction in NFSA (Figure 3A). More importantly, although IR can activate STAT1 (49, 50) it failed to do so in either FSA or NFSA cells within a 2–72 h window (Figure 7C and unpublished data). Inhibition of NLRC5 in FSA by siRNA led to an expected decrease in baseline MHC-I and a muted, but not absent, induction by IR (Figure 7A and B). Surprisingly, targeting LMP7 with siRNA increased both basal and IR-induced MHC-I levels (Figure 7A and B). How much of this relates to reactivation of NLRC5 or incomplete inhibition remains to be determined (Supplementary Figure S2D). More importantly, these results suggest that alternative or additional mechanisms may be involved in activation of NLRC5 and other members of the MHC-I APM by IR (Figure 7D). One such alternative pathway may involve NF-κB, which has long been implicated the APM activation (51–53). In support of this possibility, NF-κB inhibition by CAPE blocked IR-induced NLRC5 mRNA and MHC-I protein expression in FSA cells (Figure 7B). While the dualism between NLRC5 and NF-κB is beyond the scope of this study and may vary with cell type, it is clear that LMP7 expression has profound consequences for APM activation, tumor immunogenicity, and immune escape.

DISCUSSION

Intrinsic expression of the immunoproteasome subunits LMP7 (ß5i), LMP2 (ß1i) and Mecl-1 (ß2i), as shown here for DC2.4 dendritic cells, is generally considered a property of immune cells, although intrinsic expression by certain cancer cells has been reported (13), which may reflect their carcinogenic pathway (47, 54). The major role of immunoproteasomes expression may lie in the fact that inflammation, exemplified by IFN-γ (55), oxidative stress (56), or as we have shown previously (13), and here, by IR exposure, induces this unique exchange of three active proteolytic subunits within a chambered protease. This appears to place immunoproteasomes within a privileged place in the highly coordinated MHC-I APM that stimulates CD8+ cytotoxic T cell responses.

The importance of immunoproteasomes can also be inferred from findings that their expression in some human cancers correlates with enhanced T lymphocyte infiltration (55, 57), better prognosis (27), and response to immune checkpoint blockade (28), whereas their absence can signify poor outcomes, at least in non-small cell lung cancer (58). Conclusions from our TCGA analysis in human sarcomas showing strong correlations with CD8+ T cell infiltration and expression of other MHC-I APM members supports their pivotal role in tumor immunity. Our study confirms this by showing that murine NFSA tumors lacking LMP7 had limited intratumoral CD8+ T cells compared to FSA, but introduction of LMP7 into NFSA reversed this situation and increased tumor immunogenicity.

Loss or dysregulation of immunoproteasome expression in cancer, in particular LMP7, appears to be a tumor immune escape mechanism (27, 59–61). In some, but not all cases, immunoproteasome deficiencies can be overcome by IFN-γ treatment (62), but this was not the case for NFSA where LMP7 was not induced by either IR or IFN-γ treatment. At the same time, LMP2 was not induced by IR, but was by IFN-γ. The mechanisms underlying these effects are most likely epigenetic silencing or defects in upstream signaling

hubs as whole-exome sequencing of NFSA did not detect any non-synonymous mutations in immunoproteasome genes (Table III).

The literature on IR inducing immunoproteasomes and the coordinated APM is sparse. Gameiro et al. has also shown that IR upregulated several components of the APM, including LMP subunits, 3 days after exposure in several different human carcinoma lines (11) and Zebertavage et al. showed IR-induced NLRC5 expression along with other APM members (12). Our data in FSA indicate that 2–3 days are required for peak immunoproteasome mRNA production and that most responses last for at least 6 days. Doses of 8 or 10 Gy seem equivalent and more potent than 2 Gy, which may be relevant for findings that hypofractionation schedules tend to generate more immunity than conventional regimens (3).

Loss of inducible LMP7 expression in NFSA had knock-on effects within the coordinated APM, but there was some important divergence between IR and IFN-γ effects that suggests utilization of different pathways. For example, in this cell line, LMP2, MHC-I, and others, were induced by IFN-γ but not IR, while NLRC5, like LMP7, had muted responses to both stimuli. A cautionary note is that proLMP7 has high affinity for POMP1, accelerating proteasome assembly and increasing proteasome abundance (23, 44, 63) and this could affect proteasome subunit levels more for NFSA than FSA, even at baseline (Figure 3).

NLRC5 is a co-transactivator of the genes involved in MHC class I pathway, including HLA-A, HLA-B, HLA-C, β2-microglobulin (β2M), LMP2 and LMP7, and TAP1, and is a key player in activation of the APM (27, 34, 64). NLRC5 deficiency impairs constitutive and inducible expression of MHC class I and related genes and CD8+ T cells activation (65). This correlates with decreased CD8+ T cell infiltrates, and poor expression of immunoproteasomes and other MHC-1 APM genes (27, 66, 67). NLRC5 was induced in FSA by both IR and IFN-γ, confirming a recent report (12) and often correlates with MHC-I expression, although this may not be an absolute requirement. Firstly, in NFSA IFN-γ was able to strongly induce MHC-I with only marginal alteration in NLRC5 mRNA. Second, LMP7 gene transfer enhanced MHC-I expression without altering NLRC5 levels. Third, siRNA knock down of NLRC5 in FSA had only a limited effect on IR-induced MHC-I surface levels. Fourth, IR did not induce STAT1. The coordinated nature of the APM makes attribution of effects of loss of expression of any individual gene fraught with danger, but it seems likely that there are multiple pathways involved. However, our finding of low inducible MHC-I expression in NFSA tumors and its correction by LMP7 gene transfer agrees with the report that mice carrying a targeted deletion of LMP7 have reduced levels of cell-surface MHC-I (45), and MHC-I surface expression and tumor immunogenicity have been linked to LMP7 in the past (44, 45, 68) and confirmed here by NFSA tumor immunogenicity being restored by LMP7 gene transfer. This is reminiscent of the effects of NLRC5 gene transfer into B16-F10 melanoma driving up expression of MHC-I, immunoproteasomes, and other members of the APM (67). In this murine melanoma cell line induction of MHC-I can be uncoupled from both IFN-γ and NLRC5-signaling by NF-κB activation (51–53, 69) and this supports our observation that NF-κB inhibition by CAPE blocked all IR-induced MHC-I expression and IR is known to induce pro-inflammatory cytokines through NF-κB-dependent pathways. Ultimately, a

linear approach to understanding the network that coordinates the IP, MHC and the APM in response to different stimuli likely underestimates its complexity.

A critical issue for tumor immunity is whether immunoproteasomes are superior to standard proteasomes at producing a repertoire of epitopes for the MHC class I APM to present to CD8+ T cells for tumor regression (20, 21, 70). This is not to say that immunodominant epitopes can't be processed by standard proteasomes. In fact, many commonly used shared tumor epitopes, such as MART-$1_{27–36}$, are processed only by standard subunits (24, 25, 60, 71, 72). The IR-induced switch to immunoproteasome production described here may explain why irradiation of HLA-A2.1+ humanized dendritic cells expressing MART-1 abrogated their ability to generate MART-$1_{27–36}$ T cell responses and protective immunity (73), while RT can clearly enhance T cell-mediated immunity to many other tumor antigens (5). Our results clearly show that induced expression of LMP7 in weakly immunogenic NFSA increases its NFSA-specific immunogenicity resulting in enhanced T cell cytotoxicity and tumor regression. It is important to note that the responses are generated specifically against the unmodified NFSA tumor, as well as NFSA-LMP7, but not FSA. In other words, the epitope that is recognized is present on the original tumor, and its presentation is what matters. We came to similar conclusions using IL-3 gene transfected NFSA (38).

A critical requirement for immunoproteasome production appears to be a pro-inflammatory status, which can be generated by cytokines such as IFN-γ, IR, or oxidative and endoplasmic reticulum stresses (18, 36, 37, 56, 74). Proteasomes are extensively restructured under such conditions and there is a bias towards immunoproteasomes (75–77), perhaps because 20S immunoproteasomes are superior in rapidly recognizing and removing oxidatively damaged proteins (35, 36, 56, 74, 78) rather than for improved antigen processing. However, it is highly likely that the substrate pool for epitope processing is altered in addition to the cleavage products for the MHC-I APM. The purpose of the restructuring may also be to increase cell survival by removing toxic byproducts of stress while allowing presentation of epitopes that may generate autoimmunity in a non-immune environment (26). There are many unanswered questions relating to the use of IR within this scenario that seem important to answer if cancer RT outcomes are to improve, especially in combination with immunotherapy. Indeed, in general, immunoproteasomes may be a powerful barometer for determining if RT can make "cold" tumors "hot".

Supplementary Material

Refer to Web version on PubMed Central for supplementary material.

Acknowledgments

We thank Trent Su from the TCGB Core Facility at UCLA for his helpful advice on the WES data.

Funding:

The author is supported by the NIH with 1R01CA226875-01 (D.S.).

REFERENCES

1. McBride WH, Chiang CS, Olson JL, Wang CC, Hong JH, Pajonk F, Dougherty GJ, Iwamoto KS, Pervan M and Liao YP. 2004. A sense of danger from radiation. Radiat Res. 162: 1–19. [PubMed: 15222781]
2. Ciernik IF, Romero P, Berzofsky JA and Carbone DP. 1999. Ionizing radiation enhances immunogenicity of cells expressing a tumor-specific T-cell epitope. Int J Radiat Oncol Biol Phys. 45: 735–741. [PubMed: 10524430]
3. Schaue D, Ratikan JA, Iwamoto KS and McBride WH. 2012. Maximizing tumor immunity with fractionated radiation. Int J Radiat Oncol Biol Phys. 83: 1306–1310. [PubMed: 22208977]
4. Demaria S and Formenti SC. 2013. Radiotherapy effects on anti-tumor immunity: implications for cancer treatment. Front Oncol. 3: 128. [PubMed: 23734344]
5. Schaue D, Comin-Anduix B, Ribas A, Zhang L, Goodglick L, Sayre JW, Debucquoy A, Haustermans K and McBride WH. 2008. T-cell responses to survivin in cancer patients undergoing radiation therapy. Clin Cancer Res. 14: 4883–4890. [PubMed: 18676762]
6. Lhuillier C, Rudqvist NP, Elemento O, Formenti SC and Demaria S. 2019. Radiation therapy and anti-tumor immunity: exposing immunogenic mutations to the immune system. Genome Med. 11: 40. [PubMed: 31221199]
7. Azad A, Yin Lim S, D'Costa Z, Jones K, Diana A, Sansom OJ, Kruger P, Liu S, McKenna WG, Dushek O, Muschel RJ and Fokas E. 2017. PD-L1 blockade enhances response of pancreatic ductal adenocarcinoma to radiotherapy. EMBO Mol Med. 9: 167–180. [PubMed: 27932443]
8. Formenti SC, Lee P, Adams S, Goldberg JD, Li X, Xie MW, Ratikan JA, Felix C, Hwang L, Faull KF, Sayre JW, Hurvitz S, Glaspy JA, Comin-Anduix B, Demaria S, Schaue D and McBride WH. 2018. Focal Irradiation and Systemic TGFbeta Blockade in Metastatic Breast Cancer. Clin Cancer Res. 24: 2493–2504. [PubMed: 29476019]
9. Chen NX, Liu K, Liu X, Zhang XX and Han DY. 2020. Induction and Regulation of the Immunoproteasome Subunit beta5i (PSMB8) in Laryngeal and Hypopharyngeal Carcinoma Cells. Med Sci Monit. 26: e923621. [PubMed: 32680979]
10. Ha YJ, Tak KH, Kim CW, Roh SA, Choi EK, Cho DH, Kim JH, Kim SK, Kim SY, Kim YS and Kim JC. 2017. PSMB8 as a Candidate Marker of Responsiveness to Preoperative Radiation Therapy in Rectal Cancer Patients. Int J Radiat Oncol Biol Phys. 98: 1164–1173. [PubMed: 28721901]
11. Gameiro SR, Jammeh ML, Wattenberg MM, Tsang KY, Ferrone S and Hodge JW. 2014. Radiation-induced immunogenic modulation of tumor enhances antigen processing and calreticulin exposure, resulting in enhanced T-cell killing. Oncotarget. 5: 403–416. [PubMed: 24480782]
12. Zebertavage LK, Alice A, Crittenden MR and Gough MJ. 2020. Transcriptional Upregulation of NLRC5 by Radiation Drives STING- and Interferon-Independent MHC-I Expression on Cancer Cells and T Cell Cytotoxicity. Sci Rep. 10: 7376. [PubMed: 32355214]
13. Kim K, Brush JM, Watson PA, Cacalano NA, Iwamoto KS and McBride WH. 2008. Epidermal growth factor receptor vIII expression in U87 glioblastoma cells alters their proteasome composition, function, and response to irradiation. Mol Cancer Res. 6: 426–434. [PubMed: 18337449]
14. Leone P, Shin EC, Perosa F, Vacca A, Dammacco F and Racanelli V. 2013. MHC class I antigen processing and presenting machinery: organization, function, and defects in tumor cells. J Natl Cancer Inst. 105: 1172–1187. [PubMed: 23852952]
15. Coux O, Tanaka K and Goldberg AL. 1996. Structure and functions of the 20S and 26S proteasomes. Annu Rev Biochem. 65: 801–847. [PubMed: 8811196]
16. Baumeister W, Walz J, Zuhl F and Seemuller E. 1998. The proteasome: paradigm of a self-compartmentalizing protease. Cell. 92: 367–380. [PubMed: 9476896]
17. Demartino GN and Gillette TG. 2007. Proteasomes: machines for all reasons. Cell. 129: 659–662. [PubMed: 17512401]

18. Bose S, Brooks P, Mason GG and Rivett AJ. 2001. gamma-Interferon decreases the level of 26 S proteasomes and changes the pattern of phosphorylation. Biochem J. 353: 291–297. [PubMed: 11139393]
19. Aki M, Shimbara N, Takashina M, Akiyama K, Kagawa S, Tamura T, Tanahashi N, Yoshimura T, Tanaka K and Ichihara A. 1994. Interferon-gamma induces different subunit organizations and functional diversity of proteasomes. J Biochem. 115: 257–269. [PubMed: 8206875]
20. Gaczynska M, Rock KL, Spies T and Goldberg AL. 1994. Peptidase activities of proteasomes are differentially regulated by the major histocompatibility complex-encoded genes for LMP2 and LMP7. Proc Natl Acad Sci U S A. 91: 9213–9217. [PubMed: 7937744]
21. Akiyama K, Kagawa S, Tamura T, Shimbara N, Takashina M, Kristensen P, Hendil KB, Tanaka K and Ichihara A. 1994. Replacement of proteasome subunits X and Y by LMP7 and LMP2 induced by interferon-gamma for acquirement of the functional diversity responsible for antigen processing. FEBS Lett. 343: 85–88. [PubMed: 8163024]
22. Macagno A, Gilliet M, Sallusto F, Lanzavecchia A, Nestle FO and Groettrup M. 1999. Dendritic cells up-regulate immunoproteasomes and the proteasome regulator PA28 during maturation. Eur J Immunol. 29: 4037–4042. [PubMed: 10602014]
23. Heink S, Ludwig D, Kloetzel PM and Kruger E. 2005. IFN-gamma-induced immune adaptation of the proteasome system is an accelerated and transient response. Proc Natl Acad Sci U S A. 102: 9241–9246. [PubMed: 15944226]
24. Morel S 2000. Processing of some antigens by the standard proteasome but not by the immunoproteasome results in poor presentation by dendritic cells. Immunity. 12: 1074–1017.
25. Van den Eynde BJ and Morel S. 2001. Differential processing of class-I-restricted epitopes by the standard proteasome and the immunoproteasome. Curr Opin Immunol. 13: 147–153. [PubMed: 11228406]
26. Groettrup M, Khan S, Schwarz K and Schmidtke G. 2001. Interferon-gamma inducible exchanges of 20S proteasome active site subunits: why? Biochimie. 83: 367–372. [PubMed: 11295499]
27. Yoshihama S, Roszik J, Downs I, Meissner TB, Vijayan S, Chapuy B, Sidiq T, Shipp MA, Lizee GA and Kobayashi KS. 2016. NLRC5/MHC class I transactivator is a target for immune evasion in cancer. Proc Natl Acad Sci U S A. 113: 5999–6004. [PubMed: 27162338]
28. Kalaora S, Lee JS, Barnea E, Levy R, Greenberg P, Alon M, Yagel G, Bar Eli G, Oren R, Peri A, Patkar S, Bitton L, Rosenberg SA, Lotem M, Levin Y, Admon A, Ruppin E and Samuels Y. 2020. Immunoproteasome expression is associated with better prognosis and response to checkpoint therapies in melanoma. Nat Commun. 11: 896. [PubMed: 32060274]
29. Pajonk F and McBride WH. 2001. Ionizing radiation affects 26s proteasome function and associated molecular responses, even at low doses. Radiother Oncol. 59: 203–212. [PubMed: 11325450]
30. Pervan M, Pajonk F, Sun JR, Withers HR and McBride WH. 2001. Molecular pathways that modify tumor radiation response. Am J Clin Oncol. 24: 481–485. [PubMed: 11586100]
31. Brush JM, Kim K, Sayre JW, McBride WH and Iwamoto KS. 2009. Imaging of radiation effects on cellular 26S proteasome function in situ. International journal of radiation biology. 85: 483–494. [PubMed: 19401903]
32. Suit HD and Suchato C. 1967. Hyperbaric oxygen and radiotherapy of a fibrosarcoma and of a squamous-cell carcinoma of C3H mice. Radiology. 89: 713–719. [PubMed: 6059611]
33. Ando K, Hunter N and Peters LJ. 1979. Immunologically nonspecific enhancement of artificial lung metastases in tumor-bearing mice. Cancer Immunology, Immunotherapy. 6: 151–156.
34. Meissner TB, Li A, Biswas A, Lee KH, Liu YJ, Bayir E, Iliopoulos D, van den Elsen PJ and Kobayashi KS. 2010. NLR family member NLRC5 is a transcriptional regulator of MHC class I genes. Proc Natl Acad Sci U S A. 107: 13794–13799. [PubMed: 20639463]
35. Cardoso J, Lima Cde P, Leal T, Gradia DF, Fragoso SP, Goldenberg S, De Sa RG and Krieger MA. 2011. Analysis of proteasomal proteolysis during the in vitro metacyclogenesis of Trypanosoma cruzi. PLoS One. 6: e21027. [PubMed: 21698116]
36. Pickering AM and Davies KJ. 2012. Differential roles of proteasome and immunoproteasome regulators Pa28alphabeta, Pa28gamma and Pa200 in the degradation of oxidized proteins. Arch Biochem Biophys. 523: 181–190. [PubMed: 22564544]

37. Seifert U, Bialy LP, Ebstein F, Bech-Otschir D, Voigt A, Schroter F, Prozorovski T, Lange N, Steffen J, Rieger M, Kuckelkorn U, Aktas O, Kloetzel PM and Kruger E. 2010. Immunoproteasomes preserve protein homeostasis upon interferon-induced oxidative stress. Cell. 142: 613–624. [PubMed: 20723761]
38. McBride WH, Dougherty GD, Wallis AE, Economou JS and Chiang CS. 1994. Interleukin-3 in gene therapy of cancer. Folia Biol (Praha). 40: 62–73. [PubMed: 7958065]
39. Cancer Genome Atlas Research, N., Weinstein JN, Collisson EA, Mills GB, Shaw KRM, Ozenberger BA, Ellrott K, Shmulevich I, Sander C and Stuart JM. 2013. The Cancer Genome Atlas Pan-Cancer analysis project. Nature genetics. 45: 1113–1120. [PubMed: 24071849]
40. Cancer Genome Atlas Research Network. Electronic address, e. d. s. c. and N. Cancer Genome Atlas Research. 2017. Comprehensive and Integrated Genomic Characterization of Adult Soft Tissue Sarcomas. Cell. 171: 950–965.e928. [PubMed: 29100075]
41. Becht E, Giraldo NA, Lacroix L, Buttard B, Elarouci N, Petitprez F, Selves J, Laurent-Puig P, Sautès-Fridman C, Fridman WH and de Reyniès A. 2016. Estimating the population abundance of tissue-infiltrating immune and stromal cell populations using gene expression. Genome biology. 17: 218–218. [PubMed: 27765066]
42. Kelly A, Powis SH, Glynne R, Radley E, Beck S and Trowsdale J. 1991. Second proteasome-related gene in the human MHC class II region. Nature. 353: 667–668. [PubMed: 1922385]
43. Nandi D, Jiang H and Monaco JJ. 1996. Identification of MECL-1 (LMP-10) as the third IFN-gamma-inducible proteasome subunit. J Immunol. 156: 2361–2364. [PubMed: 8786291]
44. Joeris T, Schmidt N, Ermert D, Krienke P, Visekruna A, Kuckelkorn U, Kaufmann SH and Steinhoff U. 2012. The proteasome system in infection: impact of beta5 and LMP7 on composition, maturation and quantity of active proteasome complexes. PLoS One. 7: e39827. [PubMed: 22768135]
45. Fehling HJ, Swat W, Laplace C, Kuhn R, Rajewsky K, Muller U and von Boehmer H. 1994. MHC class I expression in mice lacking the proteasome subunit LMP-7. Science. 265: 1234–1237. [PubMed: 8066463]
46. Aptsiauri N, Cabrera T, Garcia-Lora A, Lopez-Nevot MA, Ruiz-Cabello F and Garrido F. 2007. MHC class I antigens and immune surveillance in transformed cells. Int Rev Cytol. 256: 139–189. [PubMed: 17241907]
47. Leister H, Luu M, Staudenraus D, Lopez Krol A, Mollenkopf HJ, Sharma A, Schmerer N, Schulte LN, Bertrams W, Schmeck B, Bosmann M, Steinhoff U and Visekruna A. 2021. Pro- and Antitumorigenic Capacity of Immunoproteasomes in Shaping the Tumor Microenvironment. Cancer Immunol Res.
48. Staehli F, Ludigs K, Heinz LX, Seguin-Estevez Q, Ferrero I, Braun M, Schroder K, Rebsamen M, Tardivel A, Mattmann C, MacDonald HR, Romero P, Reith W, Guarda G and Tschopp J. 2012. NLRC5 deficiency selectively impairs MHC class I- dependent lymphocyte killing by cytotoxic T cells. J Immunol. 188: 3820–3828. [PubMed: 22412192]
49. Liu S, Imani S, Deng Y, Pathak JL, Wen Q, Chen Y and Wu J. 2020. Targeting IFN/STAT1 Pathway as a Promising Strategy to Overcome Radioresistance. Onco Targets Ther. 13: 6037–6050. [PubMed: 32606809]
50. Townsend PA, Cragg MS, Davidson SM, McCormick J, Barry S, Lawrence KM, Knight RA, Hubank M, Chen P-L, Latchman DS and Stephanou A. 2005. STAT-1 facilitates the ATM activated checkpoint pathway following DNA damage. Journal of cell science. 118: 1629–1639. [PubMed: 15784679]
51. Molinero LL, Fuertes MB, Girart MV, Fainboim L, Rabinovich GA, Costas MA and Zwirner NW. 2004. NF-κB Regulates Expression of the MHC Class I-Related Chain A Gene in Activated T Lymphocytes. The Journal of Immunology. 173: 5583. [PubMed: 15494508]
52. Cheng Y, King NJC and Kesson AM. 2004. Major Histocompatibility Complex Class I (MHC-I) Induction by West Nile Virus: Involvement of 2 Signaling Pathways in MHC-I Up-Regulation. The Journal of Infectious Diseases. 189: 658–668. [PubMed: 14767820]
53. Lorenzi S, Forloni M, Cifaldi L, Antonucci C, Citti A, Boldrini R, Pezzullo M, Castellano A, Russo V, van der Bruggen P, Giacomini P, Locatelli F and Fruci D. 2012. IRF1 and NF-kB

restore MHC class I-restricted tumor antigen processing and presentation to cytotoxic T cells in aggressive neuroblastoma. PLoS One. 7: e46928. [PubMed: 23071666]

54. Koerner J, Brunner T and Groettrup M. 2017. Inhibition and deficiency of the immunoproteasome subunit LMP7 suppress the development and progression of colorectal carcinoma in mice. Oncotarget. 8: 50873–50888. [PubMed: 28881611]
55. Rouette A, Trofimov A, Haberl D, Boucher G, Lavallee VP, D'Angelo G, Hebert J, Sauvageau G, Lemieux S and Perreault C. 2016. Expression of immunoproteasome genes is regulated by cell-intrinsic and -extrinsic factors in human cancers. Sci Rep. 6: 34019. [PubMed: 27659694]
56. Johnston-Carey HK, Pomatto LC and Davies KJ. 2015. The Immunoproteasome in oxidative stress, aging, and disease. Crit Rev Biochem Mol Biol. 51: 268–281. [PubMed: 27098648]
57. Lee M, Song IH, Heo SH, Kim YA, Park IA, Bang WS, Park HS, Gong G and Lee HJ. 2019. Expression of Immunoproteasome Subunit LMP7 in Breast Cancer and Its Association with Immune-Related Markers. Cancer Res Treat. 51: 80–89. [PubMed: 29510614]
58. Tripathi SC, Peters HL, Taguchi A, Katayama H, Wang H, Momin A, Jolly MK, Celiktas M, Rodriguez-Canales J, Liu H, Behrens C, Wistuba II, Ben-Jacob E, Levine H, Molldrem JJ, Hanash SM and Ostrin EJ. 2016. Immunoproteasome deficiency is a feature of non-small cell lung cancer with a mesenchymal phenotype and is associated with a poor outcome. Proc Natl Acad Sci U S A. 113: E1555–1564. [PubMed: 26929325]
59. Singal DP, Ye M and Qiu X. 1996. Molecular basis for lack of expression of HLA class I antigens in human small-cell lung carcinoma cell lines. International Journal of Cancer. 68: 629–636. [PubMed: 8938146]
60. Joyce S 2015. Immunoproteasomes edit tumors, which then escapes immune recognition. Eur J Immunol. 45: 3241–3245. [PubMed: 26527367]
61. Miyagi T, Tatsumi T, Takehara T, Kanto T, Kuzushita N, Sugimoto Y, Jinushi M, Kasahara A, Sasaki Y, Hori M and Hayashi N. 2003. Impaired expression of proteasome subunits and human leukocyte antigens class I in human colon cancer cells. J Gastroenterol Hepatol. 18: 32–40. [PubMed: 12519221]
62. Heink S, Fricke B, Ludwig D, Kloetzel PM and Kruger E. 2006. Tumor cell lines expressing the proteasome subunit isoform LMP7E1 exhibit immunoproteasome deficiency. Cancer Res. 66: 649–652. [PubMed: 16423992]
63. Kingsbury DJ, Griffin TA and Colbert RA. 2000. Novel propeptide function in 20 S proteasome assembly influences beta subunit composition. J Biol Chem. 275: 24156–24162. [PubMed: 10816564]
64. Ludigs K, Seguín-Estévez Q, Lemeille S, Ferrero I, Rota G, Chelbi S, Mattmann C, MacDonald HR, Reith W and Guarda G. 2015. NLRC5 exclusively transactivates MHC class I and related genes through a distinctive SXY module. PLoS Genet. 11: e1005088. [PubMed: 25811463]
65. Biswas A, Meissner TB, Kawai T and Kobayashi KS. 2012. Cutting edge: impaired MHC class I expression in mice deficient for Nlrc5/class I transactivator. J Immunol. 189: 516–520. [PubMed: 22711889]
66. Chelbi ST and Guarda G. 2016. NLRC5, a promising new entry in tumor immunology. J Immunother Cancer. 4: 39. [PubMed: 27437103]
67. Rodriguez GM, Bobbala D, Serrano D, Mayhue M, Champagne A, Saucier C, Steimle V, Kufer TA, Menendez A, Ramanathan S and Ilangumaran S. 2016. NLRC5 elicits antitumor immunity by enhancing processing and presentation of tumor antigens to CD8(+) T lymphocytes. Oncoimmunology. 5: e1151593. [PubMed: 27471621]
68. Groettrup M, Kirk CJ and Basler M. 2010. Proteasomes in immune cells: more than peptide producers? Nat Rev Immunol. 10: 73–78. [PubMed: 20010787]
69. Kalbasi A, Tariveranmoshabad M, Hakimi K, Kremer S, Campbell KM, Funes JM, Vega-Crespo A, Parisi G, Champekar A, Nguyen C, Torrejon D, Shin D, Zaretsky JM, Damoiseaux RD, Speiser DE, Lopez-Casas PP, Quintero M and Ribas A. 2020. Uncoupling interferon signaling and antigen presentation to overcome immunotherapy resistance due to JAK1 loss in melanoma. Science translational medicine. 12: eabb0152. [PubMed: 33055240]

70. Goldberg AL, Cascio P, Saric T and Rock KL. 2002. The importance of the proteasome and subsequent proteolytic steps in the generation of antigenic peptides. Mol Immunol. 39: 147–164. [PubMed: 12200047]

71. Dannull J, Lesher DT, Holzknecht R, Qi W, Hanna G, Seigler H, Tyler DS and Pruitt SK. 2007. Immunoproteasome down-modulation enhances the ability of dendritic cells to stimulate antitumor immunity. Blood. 110: 4341–4350. [PubMed: 17855630]

72. Chapatte L, Ayyoub M, Morel S, Peitrequin AL, Levy N, Servis C, Van den Eynde BJ, Valmori D and Levy F. 2006. Processing of tumor-associated antigen by the proteasomes of dendritic cells controls in vivo T-cell responses. Cancer Res. 66: 5461–5468. [PubMed: 16707475]

73. Liao YP, Wang CC, Butterfield LH, Economou JS, Ribas A, Meng WS, Iwamoto KS and McBride WH. 2004. Ionizing radiation affects human MART-1 melanoma antigen processing and presentation by dendritic cells. J Immunol. 173: 2462–2469. [PubMed: 15294960]

74. Tanaka K 2009. The proteasome: overview of structure and functions. Proc Jpn Acad Ser B Phys Biol Sci. 85: 12–36.

75. Lefaki M, Papaevgeniou N and Chondrogianni N. 2017. Redox regulation of proteasome function. Redox Biol. 13: 452–458. [PubMed: 28715730]

76. Davies KJ 2001. Degradation of oxidized proteins by the 20S proteasome. Biochimie. 83: 301–310. [PubMed: 11295490]

77. Reinheckel T, Sitte N, Ullrich O, Kuckelkorn U, Davies KJ and Grune T. 1998. Comparative resistance of the 20S and 26S proteasome to oxidative stress. Biochem J. 335 (Pt 3): 637–642. [PubMed: 9794805]

78. Abi Habib J, De Plaen E, Stroobant V, Zivkovic D, Bousquet MP, Guillaume B, Wahni K, Messens J, Busse A, Vigneron N and Van den Eynde BJ. 2020. Efficiency of the four proteasome subtypes to degrade ubiquitinated or oxidized proteins. Sci Rep. 10: 15765. [PubMed: 32978409]

KEY POINTS

- IR induced immunoproteasomes and APM correlate with tumor T cell infiltration.
- Forcing LMP7 expression in a LMP7-negative tumor generates immune rejection.
- The irradiation effect on the APM is NF-kB-dependent.

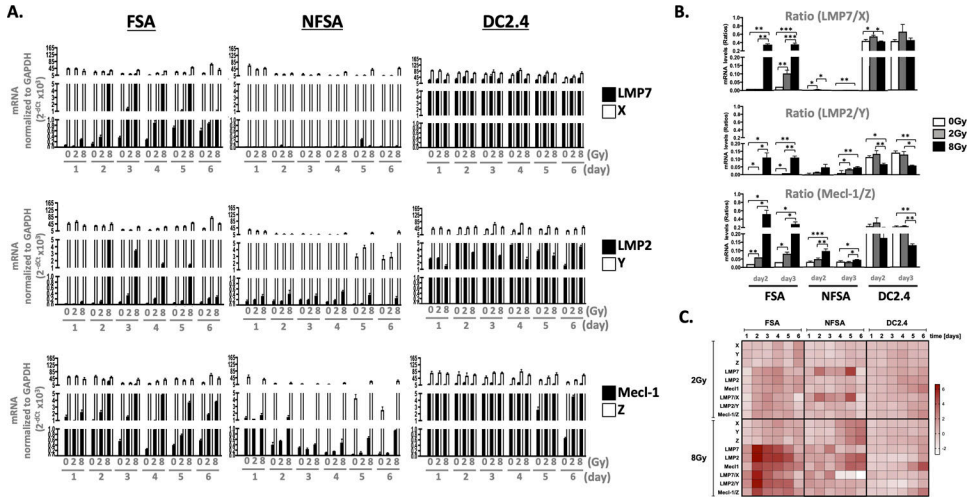

Figure 1. IR dose- and time-dependent induction of immunoproteasome expression in FSA cells with little expression in NFSA cells.

The expression of immunoproteasomes and constitutive proteasome subunits in FSA cells, NFSA cells, and DC2.4 cells with time after 0, 2 or 8 Gy IR was detected by real-time qPCR. A) Proteasome subunit levels were determined from three replicates and normalized to the average of the GAPDH mRNA levels in each sample. B) The ratios of immunoproteasome-to-constitutive β 1(Y), 2(Z), and 5(X) proteasome subunits LMP7/X, LMP2/Y, and Mecl-1/Z on days 2 and 3 after IR are presented. Note, the LMP7/X ratios for NFSA are influenced by the very low levels of LMP7 and have no biological relevance despite returning a significant T-test. C) All IR-induced changes in proteasome subunit expression are summarized in a heatmap as mean $\log_2$-fold change to 0 Gy of n=3 replicates. The experiment was repeated 4 times. *p<0.05; **p<0.01; ***p<0.001.

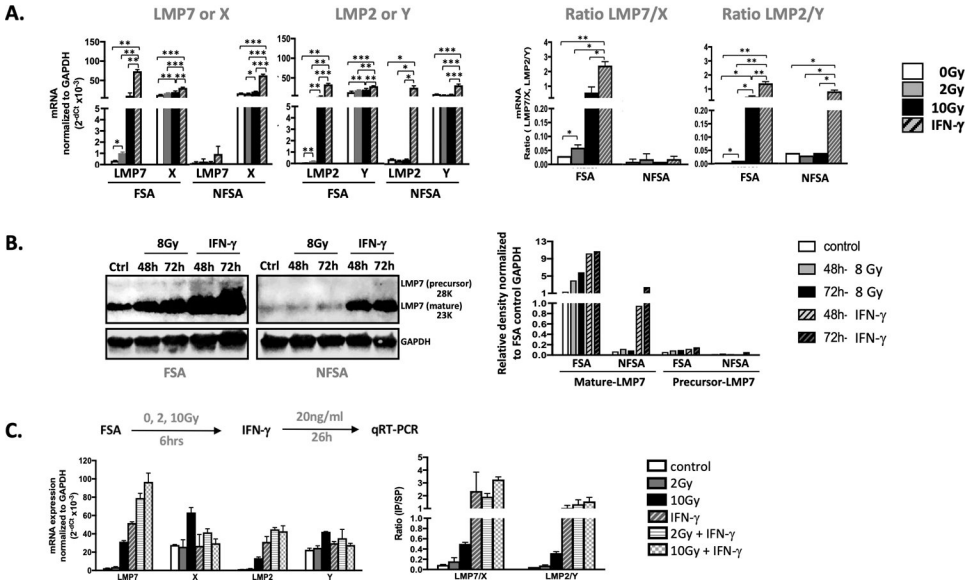

Figure 2. IR and IFN-γ treatment differentially affect immunoproteasome composition in FSA more than in NFSA cells.

A) mRNA expression of LMP7, X, LMP2 and Y were measured in FSA and NFSA cells 2 days after 0, 2, or 10 Gy IR or IFN-γ treatment (20 ng/ml) by real-time qPCR with each gene normalized to GAPDH mRNA (left) and as ratios normalized to their respective constitutive proteasomes (right). **B)** Protein levels of precursor proLMP7 and mature LMP7 in FSA and NFSA whole cell lysates untreated and after a 2–3dy treatment with either 8 Gy or 20 ng/ml IFN-γ by Western blot (left) and by densitometry normalized to GAPDH protein (right). **C)** LMP7, LMP2, X, and Y mRNA expression levels (left) and LMP7/X and LMP2/Y mRNA ratios (right) in FSA cells primed for 6hr with 0, 2, or 10 Gy followed by 26hr of treatment with 0 or 20 ng/ml IFN-γ. *p<0.05; **p<0.01; ***p<0.001.

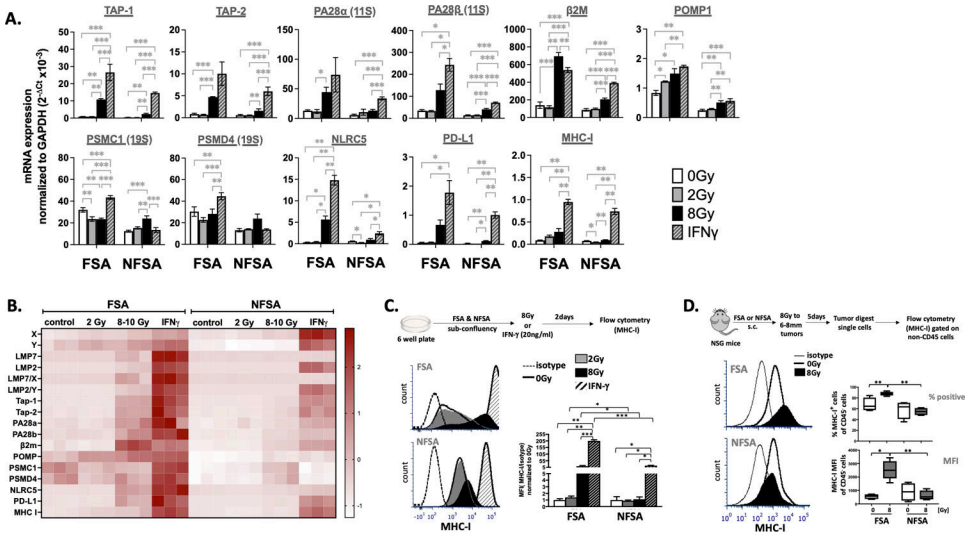

Figure 3. FSA cells are more responsive than NFSA cells to treatment-induced upregulation of proteasome subunits and components of the antigen processing and presentation machinery in vitro and in vivo.

A) The mRNA expression levels for the 11S regulatory complex subunits PA28α and β, 19S regulatory complex subunits PSMC1 and PSMD4, and POMP1, MHC-I, ß2M, TAP-1, TAP-2, PD-L1, and NLRC5 were measured by real-time qPCR in FSA and NFSA cells 2 days after 0, 2, or 8 Gy IR or IFN-γ treatment (20 ng/ml), normalized to GAPDH. (Data are mean +/− s.d.) **B)** All mRNA data on proteasome structural and regulatory subunits, and components of the antigen processing and presentation machinery and their key transcriptional activator NLRC5 before and after treatment are summarized in a heatmap after normalizing levels for each gene individually across treatments. Values are z-scores for each gene expression level in each cell line. **C)** MHC-I surface expression on FSA and NFSA cells measured by flow cytometry 2 days after in vitro irradiation with 0, 2, or 8 Gy or treatment with IFN-γ (20 ng/ml) shown as representative histograms (C, left) and as bar graphs of relative mean fluorescence intensity (MFI) (C, right) of three independent experiments. **D)** NSG mice (n=4–5) were injected s.c. with FSA or NFSA cells (0.5×10^6 cells) and, when the tumors were 6–8 mm in diameter, locally irradiated with 8 Gy. Five days after treatment, single cell tumor digests were prepared, and surface MHC-I expression on $CD45^-$ tumor cells analyzed by flow cytometry. Representative histograms are shown (D, left) and quantified as percent MHC I+ cells (D, right top) or as MFI (D, right bottom). MFI in all cases is given as MHC I antibody-to-isotype ratios. *p<0.05; **p<0.01; ***p<0.001.

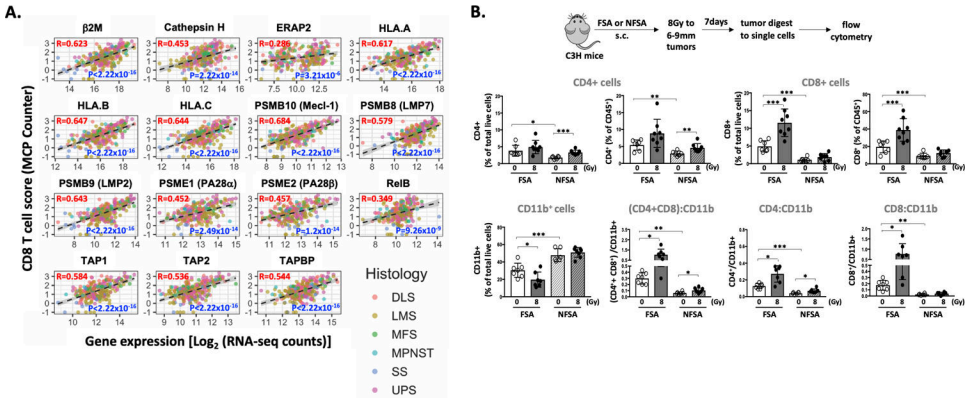

Figure 4. Expression of immunoproteasomes and APM components correlate with CD8+ T cell infiltration into human and murine sarcomas.

A) Pearson correlation analysis of immunoproteasome subunits, HLA-A, HLA-B, HLA-C, and APM expression versus the $CD8^+$ signal (RNA-seq; log-normalized counts) in sarcomas of various histological sub-types using TCGA data according to MCP-counter immune deconvolution algorithm. Data are shown in scatter blots with the Pearson correlation coefficient for each correlation superimposed in red and the p values in blue. **B)** Irradiation of FSA, but not NFSA tumors, enhanced the recruitment of tumor-infiltrating lymphocytes. 6–9mm FSA or NFSA tumors grown in the thighs of C3H mice were locally irradiated with 8 Gy and analyzed 7 days later by flow cytometry of single cell tumor digests. Major CD4+ and CD8+ immune subsets are shown as percent of all cells and as percent of $CD45^+$ (top), with CD11b+ myeloid subset and lymphoid-to-myeloid ratios highlighted (bottom). Data are means ± SD of n = 6–8. *p<0.05; **p<0.01; ***p<0.001.

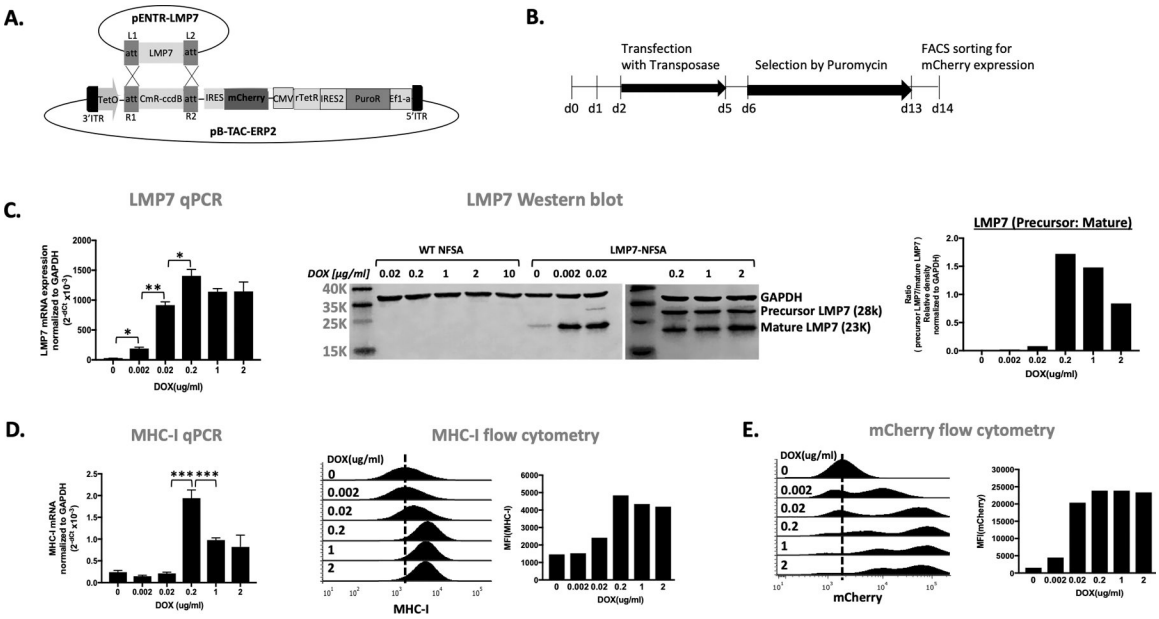

Figure 5. Forced expression of LMP7 in NFSA cells increases MHC-I expression.

A) Cloning strategy and schematic diagram of piggyBac Tet-On vector expressing mCherry and LMP7 showing the piggyBac (PB) transposon system and function of the All-in-One doxycycline-inducible expression vector: pENTR-LMP7 was moved into the An All-in-One PB vector (PB-TAC-ERP2) via Gateway LR reaction which is essentially a standard enzyme-mediated targeted recombination. The resulting vector (pB-LMP7) allows for drug inducible expression of LMP7 and tracing by an IRES-linked fluorescent reporter (mCherry) after puromycin enrichment transgenic cells. The construct is integrated into TTAA sites in genomic DNA by co-transfection with a transposase expression vector. The CMV promotor drives puromycin and a Tet repressor so that addition of doxycycline results in cells double positive for LMP7 and mCherry. **B)** Timeline of LMP7-expression cells: Transposase and pB-LMP7 were co-transfected into the target cell line using lipofectamine for 72 hours. After 72 hours, the media was changed and after 24 hours recovery, cells were selected in Puromycin for 7 days, assayed for stable pB-LMP7 integration by addition of 5 μg/mL doxycycline for 24 hours and checked for mCherry expression by FACS with the brightest 5% of mCherry expressing cells being collected. **C)** LMP7-transfected NFSA cells were treated with various concentrations of dox (0–2 μg) for 3 days and LMP7 expression measured by real-time qPCR and Western blot to determine the ratio of precursor-to-mature LMP7 protein. GAPDH served as internal control. **D)** MHC-I expression was measured by real-time qPCR and flow cytometry with **E)** confirmation of mCherry levels by flow cytometry. The data are representative of two independent experiments.

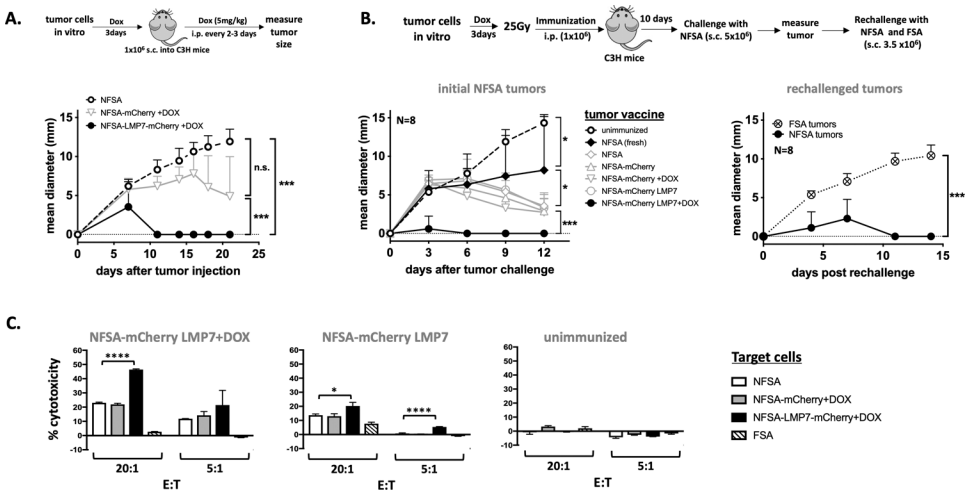

Figure 6. Overexpression of LMP7 suppresses tumor growth and improves NFSA immunogenicity yielding stronger CTL responses and tumor protection.

A) C3H mice (*n*=5 per group) were injected s.c. with 1×10^6 NFSA, or NFSA-LMP7-mCherry cells treated in vitro with and without dox (0.2 μg/ml), or dox-treated NFSA-mCherry cells. Tumor growth was measured over time with all mice being injected i.p. with dox (5 mg/kg every 2–3 days). **B)** C3H mice (*n*=8 per group) were immunized i.p. with 1×10^6 irradiated (25 Gy) NFSA, or NFSA-LMP7-mCherry or NFSA-mCherry previously treated with dox as above. Mice were challenged s.c. with 5×10^6 NFSA cells 10 days after immunization and monitored for tumor growth (B left). Non-immunized mice were used as controls, as were non-transfected NFSA and fresh NFSA cells that had been passed in vivo. Mice that rejected the NFSA challenge were rechallenged with both FSA or NFSA by s.c. injection of 3.5×10^6 tumor cells in different flanks (B right). Data are mean tumor diameters. **C)** C3H mice were immunized i.p. with 5×10^6 25Gy-irradiated NFSA-LMP7-mCherry cells that had been prior treated with (C left) or without (C middle) DOX. At day 5, splenic T cells were co-cultured with indicated target cells at effector to target (E:T) ratios of 20:1 and 5:1 and assayed for LDH release. Splenic T cells from non-immunized mice served as controls (C right). using. Data are mean percent cytotoxic activity + SD of n=3. *p<0.05; ****p<0.0001.

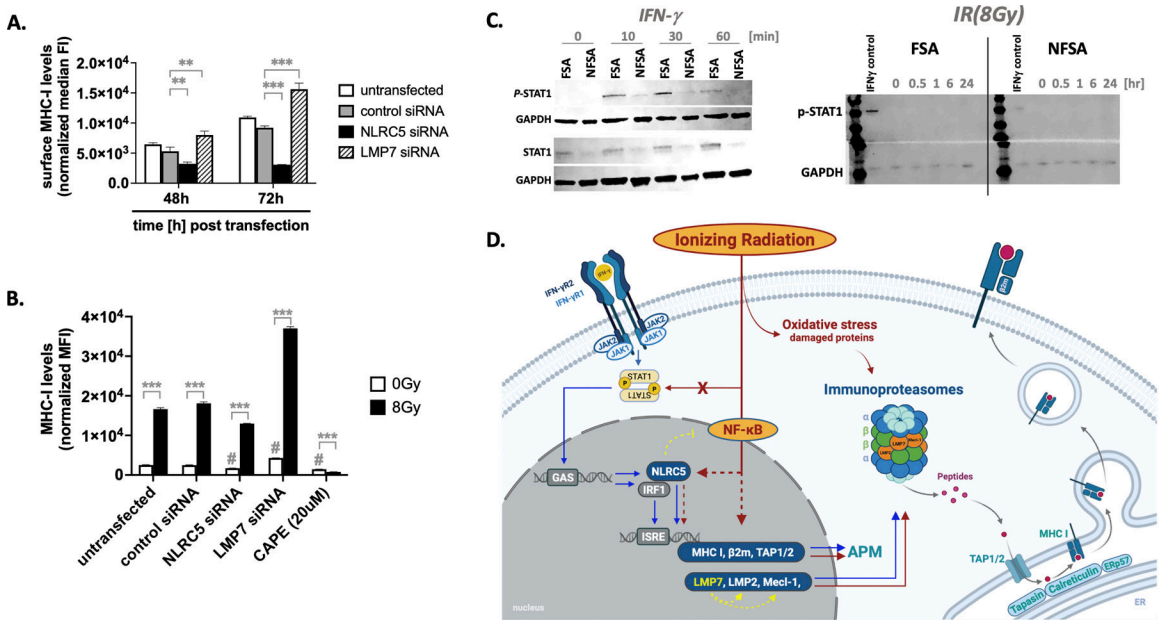

Figure 7. IR- and IFN-γ effects on the APM diverge; the role of STAT1 and NF-κB.

A) siRNA knockdown of NLRC5, but not LMP7, decreases surface MHC-I expression within 48 and 72 hours after transfection as shown as average relative median fluorescence intensity (FI) (n=3; highlighted are only differences to control siRNA **p<0.01; ***p<0.001). **B)** siRNA knockdown of NLRC5 also limited the 8Gy-induced MHC-I expression 2 days later but only to a small extent unlike what was achieved through inhibition of NF-κB with 20uM caffeic acid phenethyl ester (CAPE). Data are mean surface MHC-I mean fluorescence intensity (MFI) expression (n=3; ***p<0.001 vs each unirradiated control; #p<0.05 vs unirradiated control siRNA). **C)** FSA and NFSA cells were irradiated (0, 2, or 8 Gy) or treated with IFN-γ (20 ng/ml) and p-STAT1 and STAT1 levels assessed by Western blot at indicated time points after treatment. **D)** IR induces immunoproteasomes and the APM independently of STAT-1 activation. IFN-γ (blue arrows) and IR (red arrows) have overlapping but not identical mechanisms of action when driving antigen presentation in tumor cells. IFN-γ acts through the heterodimeric IFN-γ receptor along the canonical JAK/STAT pathway that leads to nuclear translocation of phosphorylated STAT1 dimers and binding to GAS which in turns initiates IRF1 transcription and its downstream binding to ISRE in ISGs promoter regions. With the help of the transcriptional coactivator NLRC5 numerous ISGs can be induced including those encoding immunoproteasomes subunits and members of the APM presumably optimizing the removal of oxidatively damaged proteins, and their processing and presentation on MHC-I. IR also induces immunoproteasome subunits and APM components through involvement of NLRC5 but it can do so independently from pSTAT1 utilizing NF-κB activation. Irradiated FSA tumor cells upregulate these components much more efficiently than irradiated NFSA tumor cells, which can be traced back in part to an impairment in LMP7 responsiveness in NFSA cells and suggests an upstream role for LMP7 in the hierarchy (yellow arrows). APM = antigen presentation machinery; β2m = beta-2-microglobulin; GAS = gamma-activated site; IFN-γ = interferon gamma; IRF1= interferon-regulatory factor 1; ISRE = interferon-stimulated response element; ISGs = interferon-

stimulated genes; JAK = janus activated kinase; NLRC5 = NOD-like receptor family CARD domain containing 5; TAP1/2= transporter associated with antigen processing 1 and 2; STAT1 = Signal Transducer and Activator of Transcription 1. Created in BioRender.com. *$p<0.05$; **$p<0.01$; ***$p<0.001$.

Table I:

List of mouse primers used for qPCR

Gene	Forward	Reverse
LMP2	TCACCACAGATGCCATCAC	ATCTCCCAGGATGACTCGAT
Y	AAGTCTCCACAGGGACCA	CAGAAGATGTGATCGTGGATAGG
LMP7	CAAGAAGGGACCAGGACTTTAC	CGGTAACCACTGTCCATCAC
X	TCCTGGTGATGGGCTGA	TCCATGGAGAAACTTGAAGGC
MECL-1	CGAGAACTGCCAGAGGAATG	GACTCCATCTCGGAACACAAG
Z	ATTGGTGCAGCCCTAGTTT	CCAGAACCCATGGTGACATAA
11S-PA28-α	CAACAGGAGAAGGAAGAGAAGG	TTGCAGGAGGACCACAATC
11S-PA28-β	GATGACGAGATGGAAACAGACA	GAGTCCAGACTTCTGGCTTAAC
19S-PSMC1	GAAGATGGGTCAAAGCCAGAG	TGGGACAGGAGGTTCGTATT
19S-PSMD4	CCTGCAGGGAACAGAGTTTAG	CGTCATAGTCATCCTCCTCCT
PD-L1	GAGCTGATCATCCCAGAACT	GACCGTGGACACTACAATGA
H-2Kk	TAAGGAGAGTGTGGGTGCAGA	CCGTGTTGGAGACAGTGGAT
TAP-1	CTGTTCAGGTCCTGCTCTCC	CATGTTTGAGGGTGCCAACG
TAP-2	GGGAAAAAGGGGGCCAGTTA	TCCAGTTCTGTAGGGCCTGT
β2M	CACTGAATTCACCCCCACTGA	TGTCTCGATCCCAGTAGACGG
NLRC5	GACGCTGGGGTTAACAGGAA	CAGCTCCACAAGACTCAGCA
GAPDH	TGTCAAGCTCATTTCCTGGTAT	GTGGTCCAGGGTTTCTTACTC

Table II:

siRNA sequences used for transient transfection

Target	A mixture of four validated sequences	Source	Cat#
NLRC5	CUUUGAUGGGCUACGAGUA, AAACUUGACCUGAGCCGAA, GGAAGAUGAUGGCUGUCGA GAAGUUGGCUAGCCGGAAA	Horizon Discovery	L-067620
LMP7 (PSMB8)	GUUGUAUUAUCUUCGGAAU, CUACAGUUUCUCCGCGCAA, GGACAGUGGUUACCGGCAG, GAACAAAGUGAUCGAGAUU	Horizon Discovery	L-048952
Control siRNAs	UGGUUUACAUGUCGACUAA, UGGUUUACAUGUUGUGUGA, UGGUUUACAUGUUUUCUGA, UGGUUUACAUGUUUUCCUA	Horizon Discovery	D-001810

Table III:

Annotated variants of immunoproteasomes of NFSA cells by WES

Chr	Position	Reference Base	Altered Base	AO	RO	Gene symbol	Transcript	Strand	Type	Gene section	Nucleotide change	Amino Acid change
chr17	34182168	G	A	6	2	LMP2 / Psmb9	NM_013585	-	3-prime UTR	Exon 6	c.56C>T	None
chr17	34182373	A	G	10	8	LMP2 / Psmb9	NM_013585	-	Intron	Intron 5	c.534-22T>C	None
chr17	34182381	CAAAAAAAAAAAAAAAT	CAAAAAAAAAAAAAAAAT	3	0	LMP2 / Psmb9	NM_013585	-	Intron indel	Intron 5	c.534-30GTTTTTTTTTTTTTTTA>G	None
chr17	34182421	CTTT	TTTC	8	2	LMP2 / Psmb9	NM_013585	-	Intron indel	Intron 5	c.534-70GAAA>A	None
chr17	34182488	A	G	13	6	LMP2 / Psmb9	NM_013585	-	Intron	Intron 5	c.534-137T>C	None
chr17	34182520	G	T	13	6	LMP2 / Psmb9	NM_013585	-	Intron	Intron 5	c.534-169C>A	None
chr17	34198239	CGT	CGGT	4	0	LMP7 / Psmb8	NM_010724	+	5-prime UTR indel	Exon 1	c.−160CGT>C	None
chr17	34198636	T	G	4	15	LMP7 / Psmb8	NM_010724	+	Intron	Intron 1	c.147+91T>G	None
chr17	34198776	A	G	8	0	LMP7 / Psmb8	NM_010724	+	Intron	Intron 1	c.147+231A>G	None
chr17	34198854	C	A	4	0	LMP7 / Psmb8	NM_010724	+	Intron	Intron 1	c.147+309C>A	None
chr17	34198914	T	C	9	0	LMP7 / Psmb8	NM_010724	+	Intron	Intron 1	c.149-319T>C	None
chr17	34199076	T	C	19	40	LMP7 / Psmb8	NM_010724	+	Intron	Intron 1	c.149-157T>C	None
chr17	34199077	C	T	40	20	LMP7 / Psmb8	NM_010724	+	Intron	Intron 1	c.149-156C>T	None
chr17	34199410	A	G	313	1	LMP7 / Psmb8	NM_010724	+	Intron	Intron 2	c.295+30A>G	None
chr8	105936406	C	A	2	6	Mecl-1 / Psmb10	NM_013640	-	Intron	Intron 6	c.560-259G>T	None

AO: Alternate allele observation count

RO: Reference allele observation count